Article

COVID-19 Infection Changes the Functions and Morphology of Erythrocytes: A Multidisciplinary Study

Marcos V. S. Sales,[#,a] Eloiza L. L. Tanabe,[#,b] Thamilla M. S. Maciel,[c] Maria C. Tavares,[c] Juliana G. C. Leal,[d] Larissa S. Pinto,[d] Keyla S. N. Pires,[b] Jorge A. P. M. Coelho,[e] Elaine C. O. Silva,[e] Samuel T. Souza,[e] Eduardo J. S. Fonseca,[e] Thiago S. Fragoso,[d] Thiago M. Aquino,[f] Alexandre U. Borbely,[b] Ueslen Rocha,[g] Josué C. C. Santos [*,c] and Ana Catarina R. Leite [*,a]

[a]Laboratório de Bioenergética, Instituto de Química e Biotecnologia, Universidade Federal de Alagoas (UFAL), Campus A.C. Simões, 57072-900 Maceió-AL, Brazil

[b]Laboratório de Biologia Celular, Instituto de Ciência Biológicas e da Saúde, Universidade Federal de Alagoas (UFAL), Campus A.C. Simões, 57072-900 Maceió-AL, Brazil

[c]Laboratório de Instrumentação em Química Analítica, Instituto de Química e Biotecnologia, Universidade Federal de Alagoas (UFAL), Campus A. C. Simões, 57072-900 Maceió-AL, Brazil

[d]Serviço de Reumatologia, "Hospital Clínico", Universidade Federal de Alagoas (UFAL), Campus A. C. Simões, 57072-900 Maceió-AL, Brazil

[e]Grupo de Óptica e Nanoscopia, Instituto de Física, Universidade Federal de Alagoas (UFAL), Campus A.C. Simões, 57072-970 Maceió-AL, Brazil

[f]Núcleo de Análises e Pesquisas em Ressonância Magnética Nuclear, Instituto de Química e Biotecnologia, Universidade Federal de Alagoas (UFAL), Campus A. C. Simões, 57072-900 Maceió-AL, Brazil

[g]Laboratório de Nano-Fotônica e Imagem, Instituto de Física, Universidade Federal de Alagoas (UFAL), Campus A. C. Simões, 57072-900 Maceió-AL, Brazil

Hematological problems are associated with Coronavirus disease 2019 (COVID-19). Respiratory impairment is the higher point studied, although without experimental studies related to the oxygen transport performed by erythrocytes. Therefore, we decided to investigate if erythrocytes from COVID-19 patients have their functionality changed. The case-control study included hospitalized patients with a positive real-time polymerase chain reaction (RT-PCR) result admitted to University Hospital. Volunteers (negative RT-PCR results) were recruited as a control group. Thus, we assessed different erythrocytes parameters, oxidative stress markers, and biophysical studies using whole blood and isolated hemoglobin. We found a decrease of 51% in oxygen uptake and reduced antioxidant enzyme activity in COVID-19 patients compared to controls. Raman spectrometry showed structural changes in the hemoglobin and lipids of the erythrocytes from COVID-19 patients; thus, these results were consolidated with an increase in Young's modulus in erythrocytes followed by morphology changes. Besides, isolated hemoglobin from COVID-19 patients has a distinct interaction profile using a ligand model compared to the control. COVID-19 leads to structural, functional, and morphological damage to human erythrocytes. Our data showed structural and molecular changes and induction of oxidative stress in erythrocytes by COVID-19, a new perspective on the contribution of erythrocytes to a respiratory commitment in COVID-19.

Keywords: hemoglobin, COVID-19, case-control study, red cell, morphological changes

*e-mail: *e-mail: josue@iqb.ufal.br; ana.leite@iqb.ufal.br
#The authors made an equal contribution to this work.

Introduction

Coronavirus disease 2019 (COVID-19) is caused by the Virus Severe Acute Respiratory Syndrome Coronavirus 2 (SARS-CoV-2) that has generated a pandemic situation that has persisted globally since December 2019. Data showed, at first, that people with advanced age and any comorbid disease were more susceptible to a negative outcome. Some of these concepts have changed, with the numbers showing deaths unrelated to sex, age, or comorbidities.[1-3] In this context, many questions remain with no answers, and several studies[4,5] have been presented as to how this virus can induce cell invasion or at least have a negative function in the human organism, which is a way to clarify.

In humans, COVID-19 leads, at first, to a commitment of the respiratory tract, but it also affects many other systems, such as the nervous,[1] cardiac,[2] and immunological, which in severe cases leads to cytokine storm.[3] The virus mechanism is to invade cells via receptors, such as angiotensin-converting enzyme 2 (ACE2), transmembrane protease serine 2 (TMPRSS2), and others;[4] besides, studies[5] have reported virus invasion in many cell types, such as in the reproductive system of men and in nervous cells related to smell and taste.

Coagulation complications are among the most cited pathologies associated with COVID-19 and pulmonary failure. In addition, bleeding and thrombosis were associated with the elevation of D-dimer concentration in patients with severe COVID-19.[6] Other blood dysfunctions related to COVID-19 infection are anemia and iron metabolism.[7] The hemoglobin (Hb) levels were lower in patients with increased age and affected by comorbidities. In the same way, some researchers have shown that ferritin levels are higher in the oldest hypertensive patients, which also have a high mortality rate.[8]

In this context, changes in blood homeostasis can be related to one specific cell type, in this case, the erythrocytes (Ery). However, still are limited experimental studies using Ery from blood cells infected with COVID-19; this way, many questions about the Ery alterations are without an answer. The Ery has its specificity as an oxygen transporter associated with Hb. This protein has four polypeptide chains; each contains an iron(II) ion necessary for binding to oxygen. In addition, some studies using mature COVID-19 Ery showed some changes: in antioxidant enzymes,[5] morphology (using light microscopy),[6] and structure in hemoglobin.[7,9] Recently, a study using cells erythroid precursor showed alterations in heme structure and disturbance in iron metabolism.[10]

Our research group recently presented the importance of the Ery in studies exploring alterations that showed functional and structural changes involving Hb.[11-14] In this way, in the present study, we established the hypothesis that some biochemical and biophysical parameters of red blood cells from COVID-19 patients might be altered when compared to the control group. For that, a case-control study was conducted to elucidate questions not yet clarified regarding COVID-19 infection in human Ery.

Experimental

Patients

In the present study, we employed a non-probabilistic sample (by voluntary sampling) that included 50 hospitalized adults ($\geq$ 18 years) who were positive for COVID-19 (case) and 20 negative (control) volunteers. The samples were collected from May 22nd to August 19th, 2020. Thus, the samples obtained are related to the COVID-19 first wave. The patients ranged from 25 to 94 years old, with an average age of 59.36 years old (standard deviation, SD = 15.93 years). Patients from Prof. Alberto Antunes University Hospital-HUPAA (Universidade Federal de Alagoas (UFAL), Alagoas, Brazil) were admitted to the intensive care unit (ICU) or nursery wards. The positive patients and control volunteers were confirmed by real-time polymerase chain reaction (RT-PCR) assay using a SARS-CoV-2 detection kit (Paraná Molecular Biology Institute, Brazil). The ribonucleic acid (RNA) extraction was performed using the Thermo Fisher PureLink kit (USA) for viral RNA/DNA. All clinical data were extracted from medical records, and this study was previously approved by the ethics committee (CAAE 30732120.1.0000.5013). Finally, this work followed the Strengthening the Reporting of Observational Studies in Epidemiology (STROBE) reporting guidelines for case-control studies.[15]

Clinical evaluation

The information from COVID-19 patients was collected, including medical records and laboratory results. We collected data on age, sex, chronic medical history (diabetes, hypertension, cardiovascular disease, cancer, cerebrovascular disease, chronic kidney disease, chronic pulmonary disease, chronic liver disease, and other comorbidities), clinical symptoms, respiratory support (including invasive ventilators and nasal cannula oxygen) and the outcome of the patient (discharged or died). After admission, laboratory testing was routinely performed on all patients. Routine examinations included liver and renal functions, electrolytes, complete blood count (erythrocytes; hemoglobin; hematocrit; mean corpuscular volume; mean

corpuscular hemoglobin; mean corpuscular hemoglobin concentration; erythrocytes volume distribution width; and lymphocyte, neutrophil, platelet, and monocyte counts), C-reactive protein, glucose, triglycerides, ferritin, and creatinine kinase. The biochemical (Architect, c8000, Abbott, Illinois, USA) and hematological (Cell-Dyn Ruby, Abbott, Illinois, USA) analyses were performed using specific kits for each one. We extracted data collected during admission to calculate the Quick Sequential Organ Failure Assessment (qSOFA) score. The qSOFA score comprises three clinical parameters: systolic blood pressure ≤ 100 mmHg, respiratory rate ≥ 22 breaths min^{-1}, and altered mental status.[16] The qSOFA score ranges from 0 to 3 points for each clinical variable.[17]

Chemicals

All chemicals were commercially purchased and used without further purification. Bovine serum albumin (BSA, $\geq 96\%$), ethylenediaminetetraacetic acid (EDTA, $\geq 97\%$), potassium phosphate monobasic (KH_2PO_4, $\geq 98\%$), dibasic potassium phosphate (K_2HPO_4, $\geq 98\%$), dibasic sodium phosphate (Na_2HPO_4, $\geq 98\%$), 5,5'-dithio-bis-2-nitrobenzoic acid (DTNB, $\geq 98\%$), epinephrine ($\geq 99\%$), 2-amino-2-(hydroxymethyl)-1,3-propanediol (Tris, $\geq 99.5\%$), reduced glutathione (GSH, $\geq 98\%$), glutathione reductase (GR, $\geq 98\%$), β-nicotinamide adenine dinucleotide 2'-phosphate reduced tetrasodium salt hydrate (NADPH, 97%), 8-anilino-1-naphthalenesulfonate (ANS, $\geq 97\%$), folic acid (FA, $\geq 97\%$), quercetin (QU, $\geq 95\%$), dimethyl sulfoxide (DMSO, $\geq 99.7\%$), paraformaldehyde (95%), and sodium azide (NaN_3, $\geq 99.5\%$) were purchased from Sigma-Aldrich (Saint Louis, MO, USA). Sodium chloride (NaCl, $\geq 99\%$), sodium hydrogen carbonate ($NaHCO_3$, $\geq 99\%$), sodium carbonate (Na_2CO_3, $\geq 99\%$), H_2O_2 solution (30 wt.% H_2O), acetic acid (100%), and sodium dithionite ($Na_2S_2O_4$, $\geq 86\%$) were purchased from Neon (Suzano, São Paulo, Brazil).

Blood sample collection

The blood collection from COVID-19 patients and control volunteers was performed by venous puncture with an Olen vacuum tube containing ethylenediaminetetraacetic acid tripotassium (EDTA-K3) (198 µg mL^{-1}). The virus inactivation was performed before cell separation, where the samples were submitted to 56 °C for 20 min.[18] After separating the Ery from the plasma, the blood was centrifuged at 2345 × g for 10 min at 28 °C. For the Raman spectroscopy evaluation, red blood cells were initially purified using phosphate buffer 0.2 M (pH 7.4) and

centrifuged three times at 14654 × g for 12 min at 4 °C.[11] The Ery were submitted to total protein quantification applying the Bradford method,[19] and a BSA solution (3 mg mL^{-1}) was used as a standard for total protein determination.

Oxygen uptake assay

Oxygen uptake was measured in the Ery of control volunteers and COVID-19 patients using 325 µg mL^{-1} of the protein and an oxygen electrode (OXIGY, Oxygraph+, Hansateh Instrument, Norfolk, UK) in a 1.0 mL glass chamber equipped with a magnetic stirrer. The cells were suspended in phosphate-buffered saline at pH 7.4 (PBS, 10 mM using NaH_2PO_4/Na_2HPO_4 with NaCl 100 mM), and the oxygraph electrode was calibrated daily with $Na_2S_2O_4$ to an initial oxygen concentration of 225 nmol O_2 mL^{-1} at 28 °C.[7]

Sulfhydryl group (SH) contents

The total sulfhydryl content in the samples was determined based on the reaction with DTNB. The erythrocyte homogenate (100 µg protein) was incubated in the dark with DTNB (500 µM) for 30 min. After that, the final volume was adjusted to 1.0 mL with extraction buffer (50 mM Tris-HCl with 1.0 mM EDTA, pH 7.4), and the absorbance was measured at 412 nm with a dual-beam scanning spectrophotometer (AJX-6100PC, Micronal, São Paulo, Brazil).[20]

Superoxide dismutase activity (SOD)

The Ery homogenate (80 µg protein) was incubated in 50 mM sodium carbonate buffer ($NaCO_3$/$NaHCO_3$ at pH = 10.2 with 0.1 mM EDTA) at 37 °C. The reaction was initiated by adding 20 µL epinephrine (150 mM) in acetic acid (0.05% v/v) for a final volume of 1.0 mL. The analytical signal (absorbance) was measured at 480 nm with a dual-beam scanning spectrophotometer (AJX-6100PC, Micronal, São Paulo, Brazil) for 5 min. One SOD unit was defined as the amount of protein to inhibit the autoxidation of epinephrine (1 µmol) *per* minute. The results were expressed as U mg^{-1} protein.[21]

Catalase (CAT) activity

The method principle is based on determining the decomposition of H_2O_2 in water and oxygen. A mass of 25 µg equivalent of protein (from the Ery homogenate) was added to 50 mM phosphate buffer (KH_2PO_4 + Na_2HPO_4,

pH = 7.0) at 25 °C. The reaction was started by adding 10 mM H_2O_2 to a final volume of 1.0 mL. The analytical signal decrease was monitored at 240 nm with a dual-beam scanning spectrophotometer (AJX-6100PC, Micronal, São Paulo, Brazil) for 2 min. One unit of CAT was defined as the amount of protein required to convert 1 μmol of H_2O_2 to H_2O and O_2 *per* minute. The results were expressed as K mg^{-1} protein.[22]

Glutathione peroxidase (GPx) activity

GPx activity was monitored by determining the decrease in nicotinamide adenine dinucleotide phosphate (NADPH) analytical signal at 340 nm using a scanning spectrophotometer (AJX-6100PC, Micronal, São Paulo, Brazil) for 3 min (20 °C). The system assessed contained 40 μg protein (from the Ery homogenate), 0.05 M Na_2HPO_4 (pH = 7.0), 5 mM EDTA, 84 μM NADPH, 1.1 mM sodium azide, 1.5 mM GSH, 0.1 U GR, and 90 μM H_2O_2 in a final volume of 1.0 mL. One enzyme unit was defined as the amount required for the oxidation of 1 μmol of NADPH min^{-1} mg^{-1} of protein. Finally, the results were expressed as U mg^{-1} protein.[23]

Biophysical studies

Hb was obtained by collecting blood from COVID-19 patients (n = 45) and control volunteers (n = 18). The human Hb solution was prepared from a pool of three samples and protein quantification according to previously described procedures ("Blood sample collection" sub-section). The other reagents used in this work were of analytical grade with a minimum purity of 95%. ANS and FA stock solutions were prepared in DMSO, while QU was in ethanol, and the subsequent dilutions were performed in 10 mM phosphate buffer solution (10 mM, pH = 7.4 ± 0.1). Shimadzu RF spectrofluorimeter (5301PC, Shimadzu, Osaka, Japan) was used for the spectrofluorimetric measurements, which were performed in the steady-state mode maintained the Hb at 325 μg mL^{-1} (λ_{ex} = 280 nm) and increased the concentration of FA or QU (2.5-50 μM). Mathematical corrections in the data were applied when necessary to eliminate the internal filter effect. All measurements were performed at room temperature (25 °C). For the three-dimensional (3D) fluorescence study, the fluorescence 3D emission spectra of Hb (325 μg mL^{-1}) were used in the absence and presence of the ligands (FA or QU). The spectra were recorded by exciting the protein from 220 to 450 nm and monitoring emission in the interval of 250-500 nm.[13] The synchronized fluorescence measurements were obtained by simultaneous variation of emission and excitation monochromators,

applying $\Delta\lambda$ = 15 and $\Delta\lambda$ = 60 nm to monitor the tyrosine (Tyr) and tryptophan (Trp) residues, respectively.[24] The ANS probe (4 μM) was used to assess the Hb external hydrophobicity sites ($\lambda_{ex}/\lambda_{em}$ = 360/475 nm).[25] The spectrofluorimetric measurements were performed using excitation and emission slits of 5 and 10 nm, respectively, while spectrophotometric measurements were performed on a dual-beam scanning spectrophotometer (AJX-6100PC, Micronal, São Paulo, Brazil). The absorption spectra of free Hb (65 μg mL^{-1}) were recorded from 200 to 500 nm in phosphate buffer 10 mM (pH = 7.4).[13] For discrimination based on principal component analysis (PCA), in each spectrum was applied a first-order derivative associated with a Savitzky-Golay smooth (polynomial order = 1, points of window = 5). Finally, the score plot was designed using blood samples from COVID-19 patients (n = 25) and control volunteers (n = 20).

Raman spectroscopy of Ery

Ery from COVID-19 patients and control volunteers were placed under a silicon plate at 211.2 ± 3.2 μg of total protein, and a microscope (LabRam HR Evolution, Horiba, Austin, USA) was used. For spectral measurements, a 100× objective lens (Olympus IR, Bartlett, USA) was employed with a 785 nm laser for excitation and 40 s accumulation time. Alternatively, a 532 nm laser was used for the comparison of results. All spectra were registered between 300 and 1800 cm^{-1} and measured at 28 °C. The spectra were normalized using the vibrational band of standard silicon 520 cm^{-1} as a reference. In addition, to discriminate between COVID-19 patients and control volunteers, PCA and unsupervised chemometric analysis were used.

Atomic force microscopy measurements

Before acquiring atomic force microscopy (AFM) data, the samples from COVID-19 patients (case) and control volunteers were prepared by processing the Ery (350 μg protein mL^{-1}) in a fixed 1:1 solution of paraformaldehyde and phosphate-buffered saline (10 mM to NaH_2PO_4/Na_2HPO_4 containing NaCl 100 mM). Next, according to the manufacturer's descriptions, a small amount of the Ery had adhered with poly-L-lysine (PLL, Bio-techne, US) on the sterilized round glass. Then, the cellular morphology images and elasticity measurements were obtained using a standard AFM setup (Multiview 4000™, Nanonics, Israel) with a combined optical microscope (BXFM, Olympus, Tokyo, Japan). Thus, this combination permitted AFM tip over the nuclear region of the cell with micrometer-scale precision using lateral positioning.

Furthermore, to reduce interference noise in the ambient during the measurements, the AFM system was acoustically isolated; besides, the equipment was secured on an active damping table to suppress mechanical noise. Cell topography was imaged in tapping mode with a scan rate of 0.2 Hz, and the AFM images were processed with WS×M software 9.[26] The AFM images were carried out using a scanning tip with a typical radius of curvature < 10 nm and a nominal frequency of 35 kHz. The scanned areas were 80 μm × 80 μm, and the morphology for 25-35 cells (an average of 90 cells for the group) was analyzed on each scan. Using a tip with a typical radius of curvature < 20 nm and a spring constant of < 1 N m^{-1}, the experiments were performed. The cantilever's spring constant was calibrated by fitting the power spectrum to a simple harmonic oscillator,[27] and the maximum indenting force for the cantilever was set at 40 nN. Force-distance curve measurements were performed by moving the cantilever tip toward the sample with a constant load speed of 5 μm s^{-1}. Finally, 100 force-distance curves were acquired for each group of cells COVID-19 infected (n = 5) and control (n = 5). All force-distance curve experiments were performed with the same tip.

Statistical analysis

Data represent the mean ± standard error (SE) or mean ± standard deviation (SD) of the experimental results. In the AFM experiments, data were normally distributed (Shapiro-Wilk assay). The statistical significance of the differences between COVID-19 patients and control volunteers was evaluated using a two-sample independent Student's *t*-test (at a 95% confidence level, $p < 0.05$). To analyze the groups' variations and whether any clinical or experimental data had statistical significance, we performed descriptive (frequency, percentage, mean, standard deviation, and mean difference). Finally, the decision-making through independent Bayesian samples and *t*-tests to compare the mean scores of the studied groups was performed (at a 95% confidence level, $p < 0.05$).

Results

Our work is based on COVID-19 patients admitted at HUPAA from May 2020 to August 2020. The initial analysis of volunteers (infected and control groups) verified that more women than men (56%) were admitted directly to the ICU (48%), and almost half of them had a negative outcome (46%), in this case, death (Table 1). The statistic evaluation of results was performed using the Bayesian approach, widely used in case-control epidemiological studies and provides additional advantages against classic hypothesis tests.[28] The

results of the Bayes Factor (BF$_{10}$) could be attributed to three distinct categories: (*i*) evidence in favor of alternative hypothesis H$_1$ (presence of one effect); (*ii*) evidence in favor of null hypothesis H$_0$ (absence of one effect); and (*iii*) evidence that favors neither the H$_1$ nor the H$_0$ hypothesis.[29]

In front of this, it was evidenced that the Hb, hematocrit (HCT), lymphocyte, C-reactive protein (CPR), and oxygen uptake parameters are strongly associated with the alternative hypothesis (H$_1$) based on the BF$_{10}$ values between the COVID-19 and control volunteer groups for a 95% confidence interval. In the same way, the ferritin concentration was moderately in agreement with the H$_1$ hypothesis (Table S1, Supplementary Information (SI) section). Additionally, the magnitude of the effect on group separation was calculated based on Cohen's *d*,[30] and it was observed that the Hb, HCT, lymphocyte, CPR, and oxygen uptake parameters presented a strong influence (*t*-test for the 95% confidence interval) for separation between groups, while Ery and ferritin parameters indicated a medium effect (Table S1). When evaluating the outcomes of COVID-19 patients (death or medical discharge) using the clinical, biochemical, and hematological parameters, no difference was observed between the groups (Table S2, SI section) using the statistical analysis (at 95% confidence interval) based on the BF$_{10}$ and Cohen's *d* values. Finally, some statistical analyses were performed for separated groups using the criteria of gender, age, and comorbidities; however, no differences between the groups were found in the possibilities assessed.

In order to assess the primary function of Ery, a decrease of about 51% in oxygen uptake in cells from COVID-19 patients (case) compared to controls was found (Figures 1a-1b). Moreover, a systematic reduction in the activity of antioxidant enzymes assessed was found, in this case, SOD (28%), CAT (83%), and GPx (39%) (Figures 1c-1e), which probably indicates an oxidative stress condition of these Erys. In contrast, the sulfhydryl group content (a secondary marker of reactive oxygen species, ROS) did not differ between the groups at a 95% confidence interval (Figure 1f).

Biophysical interaction studies were performed to assess conformational changes of the Hb in blood samples from COVID-19 patients compared with the control. Thus, some parameters were obtained from the interaction of the iron protein with two model ligands, folic acid (FA or vitamin B9, associated with immunity) and quercetin (QU, antioxidant compound) (Figure S1, SI section). The addition of the ligands (FA or QU) resulted in a gradual decrease in the fluorescence intensity of Hb (Figures 2a and S2a, SI section) due to forming a non-fluorescent complex (Hb-FA

Table 1. Clinical characteristics of COVID-19 (case) patients and control volunteers

Characteristic		Control group (n = 20)	COVID-19 group (case) (n = 50)
Age (mean ± SD)		58 ± 12	60 ± 17
Sex[a] / number	male	9 (45)	22 (44)
	female	11 (55)	28 (56)
Comorbidities[a] / number	hypertension	8 (40)	28 (56)
	diabetes	2 (10)	24 (48)
	cancer	0 (0)	18 (36)
Admission[a] / number	nursery	–	26 (52)
	ICU	–	24 (48)
Outcome[a] / number	death	–	23 (46.0)
	discharge	–	27 (54.0)
Biochemistry (mean ± SD)	Ery / (10^6 mm^{-3})	4.67 ± 0.39	4.19 ± 0.86
	Hb / (g dL^{-1})	14.1 ± 1.1	12.0 ± 2.4
	HCT / %	42.1 ± 3.0	36.6 ± 6.8
	MCV / fl	90.3 ± 4.0	87.8 ± 6.9
	MCH / (u mL^{-1})	30.3 ± 1.4	29.1 ± 2.7
	MCHC / %	33.5 ± 0.5	33.2 ± 1.7
	RDW / %	13.6 ± 0.6	12.8 ± 2.0
	oxygen uptake / (nmol O_2 mg^{-1} min^{-1})	185 ± 56	88.1 ± 54.4
	lymphocytes / (10^6 mm^{-3})	2243 ± 564	1334 ± 974
	glucose / (mg dL^{-1})	121 ± 54	194 ± 126
	triglycerides / (mg dL^{-1})	177 ± 114	334 ± 456
	ferritin / (ng mL^{-1})	194 ± 131	2456 ± 3586
	CRP / (mg L^{-1})	2.90 ± 2.60	141 ± 122
	CK / (u L^{-1})	169 ± 97	346 ± 663

[a]Values in parenthesis represent the percentage (%). The parameters: oxygen uptake, glucose, triglycerides, ferritin, and CK, correspond respectively to n = 43, 38, 31, 46, 39 to COVID-19 infected patients. COVID-19: Coronavirus disease 2019; SD: standard deviation; Ery: erythrocytes; Hb: hemoglobin; HCT: hematocrit; MCV: mean corpuscular volume; MCH: mean corpuscular hemoglobin; MCHC: mean corpuscular hemoglobin concentration; RDW: red cell volume distribution width; CRP: C-reactive protein; CK: creatinine kinase; ICU: intensive care unit.

or Hb-QU).[31] From the spectrofluorimetric titrations, Stern-Volmer constants (K_{SV}) related to the quenching process and the binding constant (K_b), which indicates the magnitude of the macromolecule-ligand interaction, were obtained from equations 1 and 2, respectively:

$$\frac{F_0}{F} = 1 + K_{SV}[L] \qquad (1)$$

$$\log\left[\frac{(F_0 - F)}{F}\right] = \log K_b + n\log[L] \qquad (2)$$

where F_0 and F are the fluorescence intensities in the absence and presence of ligands (L), K_{SV} is the Stern-Volmer constant obtained from the angular coefficient of linearization F_0/F *vs.* [ligand]. K_b and n (number of binding sites) values were obtained by linear regression from $\log[(F_0 - F)/F]$ *vs.* log[ligand].

For both ligands (FA and QU), the K_{SV} values for the control were higher than the virus-infected group (Figures 2b and S2b), indicating that the fluorophore was not accessible to the ligands in the COVID-19 group, probably due to structural changes in Hb. However, in the presence of FA, the binding constant (K_b) values were higher for the control compared to the infected patients (Figure 2c), while for QU, the opposite was observed (Figure S2c). Although each ligand assessed presented a typical profile, both indicate that the presence of SARS-CoV-2 possibly causes changes in the structure of Hb, evidenced by the higher or lower affinity of the protein with the model ligand compared to the control. Finally, the values of n were statistically similar ($\alpha = 0.05$) since they were equal to 1.07 ± 0.11 (control) and 1.15 ± 0.13 (COVID-19).

Synchronous fluorescence is used to explore changes in the Tyr ($\Delta\lambda = 15$ nm) and Trp ($\Delta\lambda = 60$ nm) residue
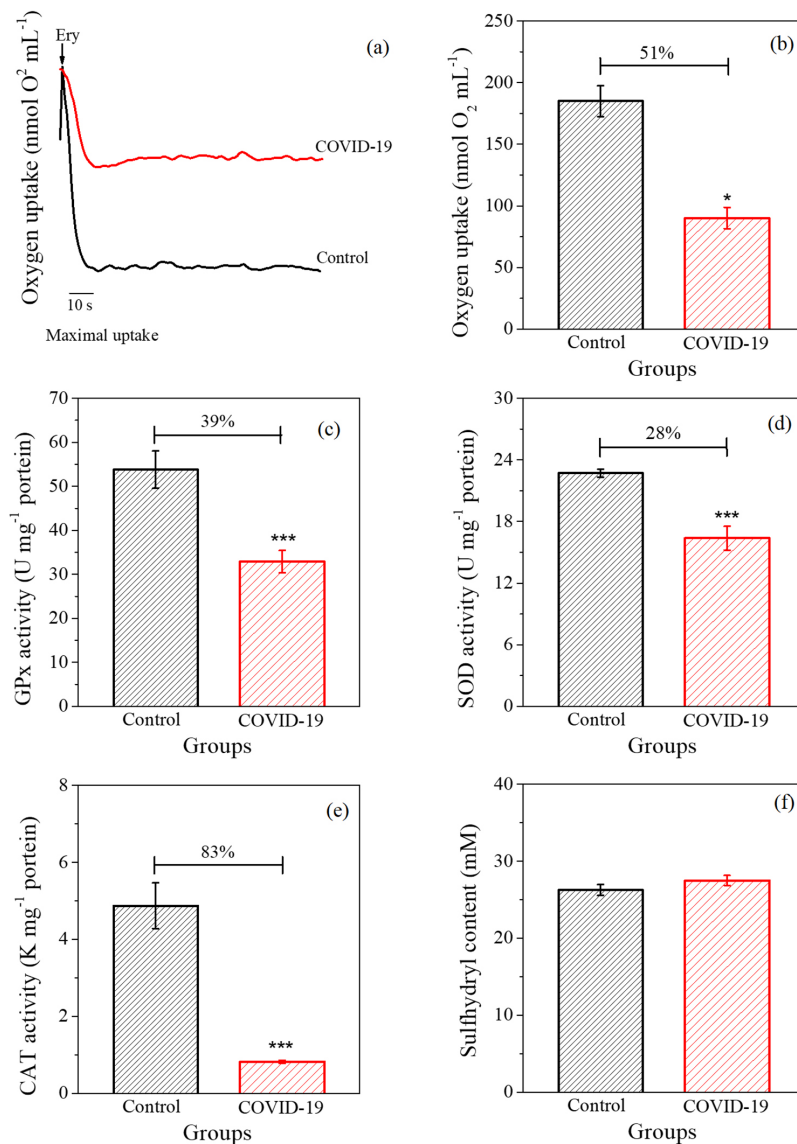
Figure 1. Function and redox state of Ery from COVID-19 (case, n = 50) and control patients (n = 20). (a) Representative experiment of O_2 uptake at 28 °C. (b) Quantification of O_2 uptake, ***$p < 0.0001$; (c) glutathione peroxidase activity (GPx, control: 53.8 ± 4.2 *vs.* COVID-19: 32.9 ± 2.5 U mg^{-1} protein, ***$p < 0.0001$); (d) superoxide dismutase activity (SOD, control: 22.7 ± 0.4 *vs.* COVID-19: 16.4 ± 1.2 U mg^{-1} protein, ***$p = 0.0005$); (e) catalase activity (CAT, control: 4.87 ± 0.59 *vs.* COVID-19: 0.82 ± 0.04 K mg^{-1} protein, ***$p < 0.0001$). (f) Quantification of total free thiol content (expressed in cysteine equivalents). Data represent independent experiments carried out in duplicate. Statistical analysis using Student *t*-test for unpaired samples and mean ± SE.

microenvironments in proteins.[32] For both ligands, FA or QU, it was observed that the K_{SV} values showed a significant difference compared to the control with the infected group. These results indicate that the Tyr and Trp microenvironments are affected by a virus infection (Figures 2d-2e and S2d-S2e, SI section). Three-dimensional fluorescence (3D) was used to evaluate conformational changes in protein structure.[13,33] The Stokes shift ($\lambda_{ex} - \lambda_{em}$) for the aromatic amino acids (mainly Tyr and Trp) was higher for the COVID-19 patients (42.1 ± 5.2 nm) compared to the control group (25.5 ± 2.1 nm) (Figure 2f). The ANS probe assesses protein surface hydrophobicity;[26,27] thus, the fluorescence intensity of the ANS-Hb complex was

higher for the control group (410 ± 62 a. u.) compared to the infected groups (216 ± 48 a. u.) (Figure 2g). This result indicated that the virus could cause changes in the protein surface and decrease the ability of the probe to bind to the Hb surface.

The Hb absorption (240-490 nm) spectrum has two characteristic absorption bands ($\pi \rightarrow \pi^*$ transitions) at 276 and 412 nm, which refer to the aromatic amino acid residues and the Soret band (heme group), respectively.[13] This study evaluated the Soret band for separate control and infected groups based on the chemometric evaluation. The intensity of the Soret band absorption varied between groups (Figure 2h), thus allowing discrimination between
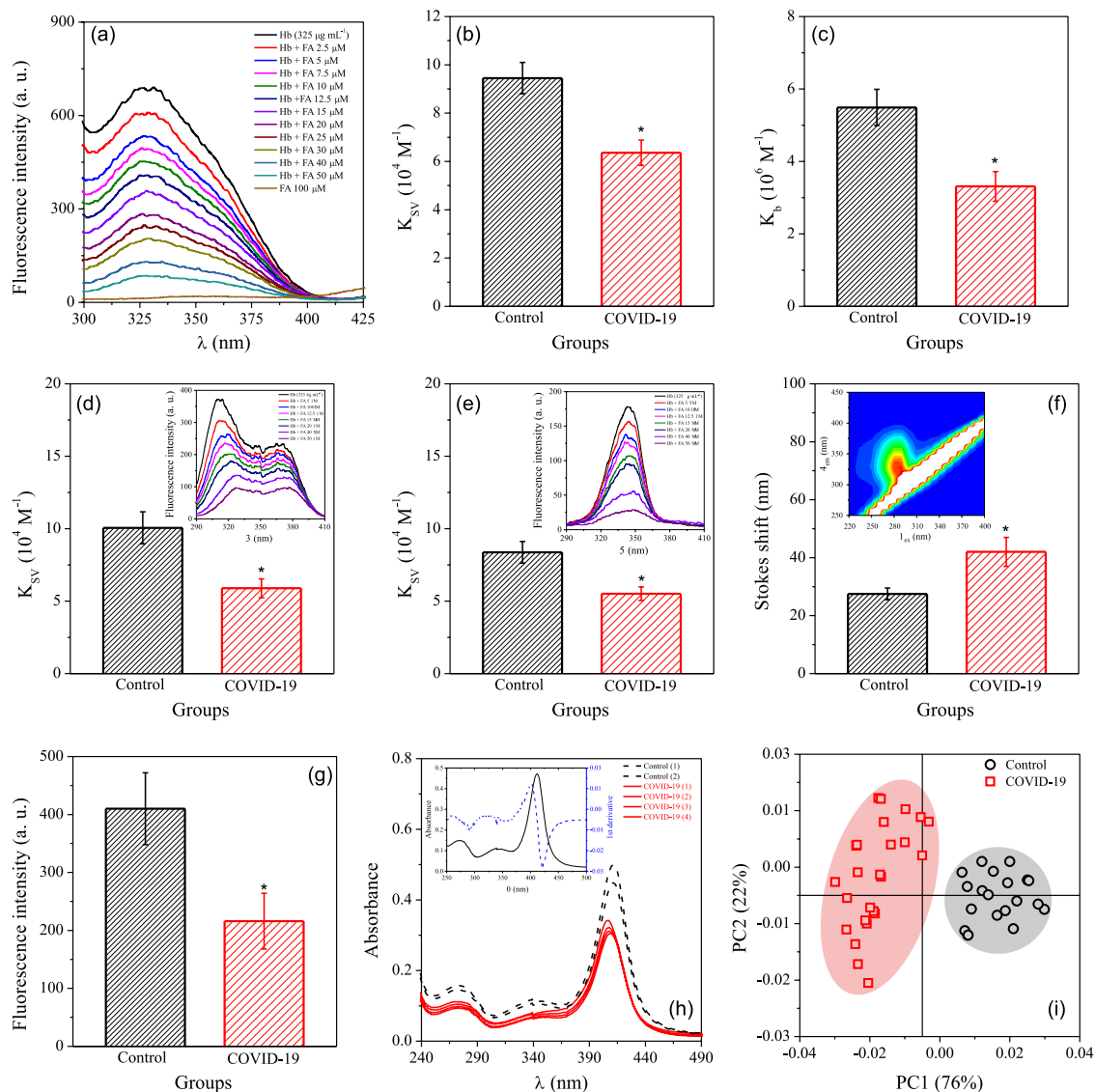
Figure 2. Biophysical studies employing Hb from blood samples from COVID-19 patients (case, n = 45) compared to control volunteers (n = 18) using folic acid as a model ligand. (a) Spectrofluorimetric titration profile of Hb (control, 325 µg mL⁻¹) with folic acid; (b) Stern-Volmer constant of Hb with FA (K_{SV}, control: 9.45 (± 0.65) *vs.* COVID-19: 6.36 (± 0.52) × 10⁴ M⁻¹); (c) binding constant of Hb with FA (K_b, control: 5.49 (± 0.50) *vs.* COVID-19: 3.31 (± 0.41) × 10⁶ M⁻¹); (d) synchronous fluorescence titration for Tyr residues of Hb with FA (insert: spectrofluorimetric titration profile, $\Delta\lambda = 15$ nm) (K_{SV}, control: 10.06 (± 1.10) *vs.* COVID-19 : 5.89 (± 0.65) × 10⁴ M⁻¹); (e) synchronous fluorescence titration for Trp residues of Hb with FA (insert: spectrofluorimetric titration profile, $\Delta\lambda = 60$ nm) (K_{SV}, control: 8.37 (± 0.75) *vs.* COVID-19 : 5.51 (± 0.47) × 10⁴ M⁻¹); (f) Stokes shift from three-dimensional fluorescence of Hb (insert: 3D spectra of control Hb) (control: 25.5 ± 2.1 *vs.* COVID-19 : 42.1 ± 5.2 nm); (g) fluorescence intensity of the complex Hb-ANS (control: 410 ± 62 *vs.* COVID-19 : 216 ± 48 a. u.); (h) UV-Vis spectral profile of some blood samples of COVID-19 and control with Hb a 65 µg mL⁻¹ (insert: spectrum first-order derivative of control blood sample), and (i) PCA analysis. Score graph from discrimination of the COVID-19 and control volunteer groups using UV-Vis spectral information. An independent Student's *t*-test was used to compare the results with a statistical significance of $p < 0.05$ (*).

the COVID-19 and control groups using the first derivative of the Hb spectrum since PC1 + PC2 was capable of explaining 98% of the total system variation (Figure 2i). Thus, proving that there is a variation in the Hb structure of COVID-19 patients compared to the control volunteers and corroborated with the O₂ uptake studies (Figures 1a-1b).

Raman spectroscopy was used to investigate structural changes in Hb. Thus, the average normalized spectra of red blood cells from the COVID-19 patients (case) were compared to the control group using a 785 nm laser with

excitation to 300-1800 cm⁻¹ (Figure 3a). The major Raman bands of Ery were assigned by vibrational modes of Hb, including the oxygenated or deoxygenated hemoglobin porphyrin ring and amino acids: Fe^{II}–O₂ (564 cm⁻¹), pyrrole ring vibrations (676 and 755 cm⁻¹), CH deformation vibrations probably from amino acids (950 cm⁻¹), phenylalanine vibrations (1004, 1031, and 1076 cm⁻¹), CN deformation vibrations (1129 cm⁻¹), pyrrole ring stretching vibration region (1400-1300 cm⁻¹), and CH deformation vibrations from lipids (1225 cm⁻¹); the band assignments
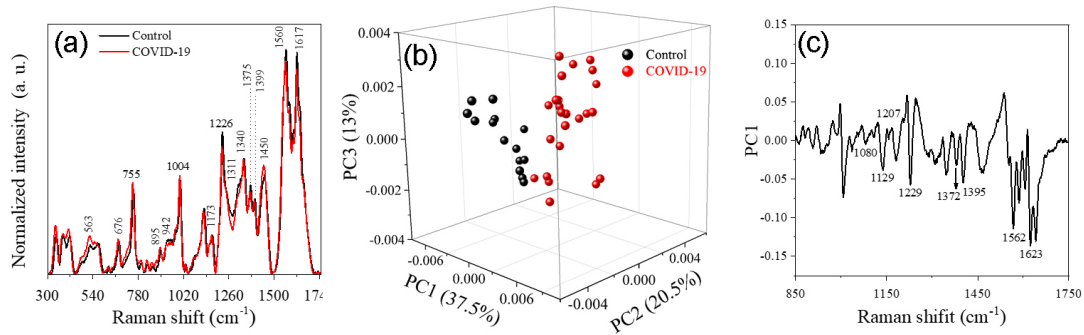
Figure 3. Raman spectra profile. (a) Mean spectra of Ery in the spectral range from 300-1800 cm^{-1} using a 785 nm laser for excitation. (b) PCA at three-dimensional score applied to Raman spectra obtained under 785 nm laser excitation of Ery, showing general separation between the healthy volunteers (control: black dots) and unhealthy volunteers (infected with COVID-19: red dots). (c) Loading profile of PC1.

and coordinates are summarized in Table S3 (SI section).

A 3D PCA graphic score shows discrimination between the control volunteers (n = 15) and COVID-19 patients (n = 26), explaining 71.1% of the total variance (PC1 + PC2 + PC3) for the 785 nm laser (Figure 3b). Finally, the loading profile from PC1 to 785 nm (Figure 3c) was used for the Raman fingerprint vibrational assignments between Ery from the COVID-19 and control groups. Similar results were found using 532 nm laser excitation (see SI section).

In front of these results, we decided to evaluate cell microscopy considering biophysical spectroscopy results, where modifications in hemoglobin and membrane lipid were evidenced. Thus, AFM measurements were performed in Ery from the control and COVID-19 groups to investigate structural and biomechanical properties alterations (Figures 4a-4b). The average width (diameter) and thickness (height) of the Ery were

determined (Figures 4c-4e) using linear regression. The mean values of the Ery from control volunteers were 8.92 ± 0.73 μm (diameter) and 1.27 ± 0.11 μm (height), while Ery from COVID-19 patients presented a diameter of 10.41 ± 0.78 μm and height of 0.98 ± 0.07 μm. Furthermore, the groups' histograms of frequency *vs.* diameter for Ery demonstrated Gaussian distribution fits (Figure 4e). The morphological analysis indicated that Ery from COVID-19 patients showed differences in diameter and height mean values compared to the control. Overall, COVID-19-infected RBCs increased by 14% in diameter and decreased by 30% in height compared to Ery from the control.

Ery stiffness (Young's modulus) was obtained from measurements of a random set in each sample by AFM force curves (Figure 4f). The stiffness of the Ery increased up to 74% for COVID-19 patients compared to control patients. Figure 4g presents the histograms obtained for
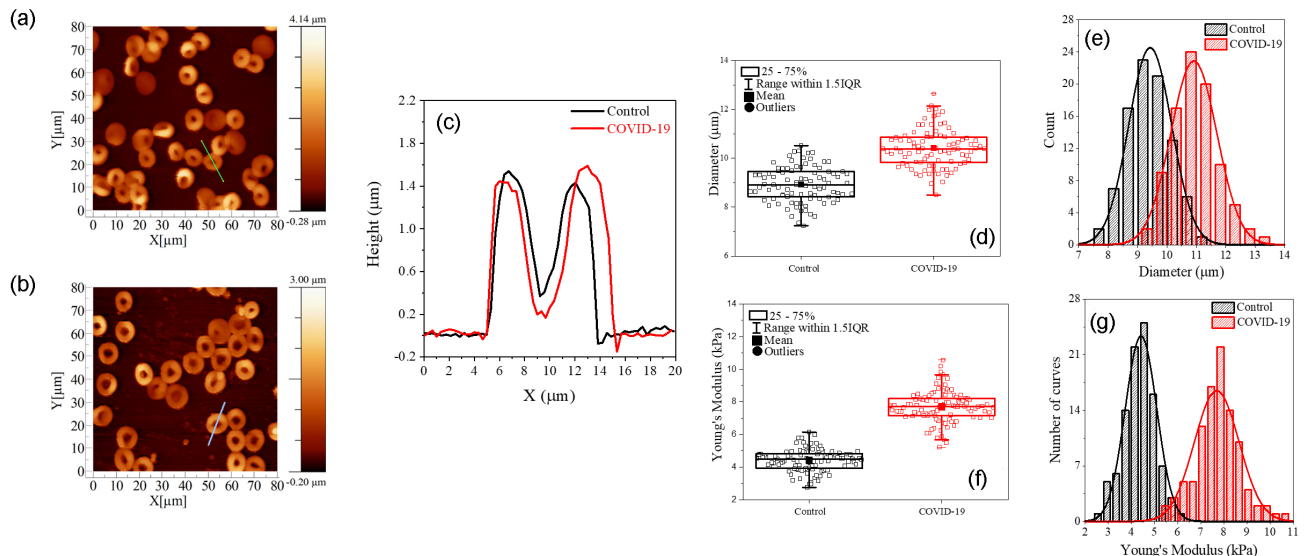

Figure 4. Atomic force microscopy (AFM) images of cells (a) control and (b) COVID-19 patients. (c) Distribution of the cells concerning the parameters of diameter and height for both diameter and height. (d) Box plots of the diameter of cells. The average diameter is shown by the horizontal line within each box, $p < 0.0001$. (e) Number of curves *vs.* Ery diameter from control and COVID-19 patients; (f) box plots of Young's moduli of cells from control and COVID-19 patients, $p < 0.0001$. (g) Number of curves *vs.* Young's moduli of Ery from control and COVID-19 patients. The horizontal line within each box shows the average Young's modulus. One-sample independent Student *t*-test was applied ($p < 0.05$).

the control and COVID-19 groups, and the average values of Young's modulus were 4.41 ± 0.68 kPa (control) and 7.69 ± 0.10 kPa (COVID-19).

Discussion

When we analyzed the clinical parameters of the control volunteers against the COVID-19 patients, a statistically significant difference was observed between the Hb, HCT, lymphocyte, CRP, ferritin, and O_2 uptake parameters. Furthermore, the Hb, HCT, and O_2 uptake parameters are directly related to Ery functionality, which is compromised in COVID-19 patients. In addition, CRP is a protein marker associated with an inflammatory process associated with this disease.[34]

Although some relevant clinical parameters found in this study are associated with respiratory function, specifically invasive ventilation and nasal cannula oxygen, the inflammatory parameters (lymphocytes and CRP) showed that COVID-19 patients, independent of comorbidities, have a negative outcome. However, these results are not a novelty since some groups worldwide have already published these findings of COVID-19 infection.[35,36] The innovation of our results is based on the differences in some clinical parameters related to Ery (Hb, HCT, and ferritin), which was the cell chosen for our deep investigation. In contrast to these hematological findings, Thomas *et al.*[37] analyzing 29 COVID-19 and 23 control volunteers, found no difference between the groups in most parameters, like Ery count, hematocrit, or mean corpuscular hemoglobin concentration.

When we used some statistical approaches to compare the biochemical and hematological parameters of SARS-CoV-2-infected patients to the control group, it was evidenced that the Hb, HCT, lymphocyte, CRP, and oxygen uptake parameters favor the alternative hypothesis (H_1), indicating a high difference between the COVID-19 and control groups to a 95% confidence interval. In contrast, ferritin concentration favors H_1 with a moderate mode (Table S1, SI section). Finally, to assess the possibility of establishing a prognosis based on clinical, hematological, and biochemical data, patients infected with COVID-19 were compared with those with different outcomes (medical discharge or death). For this comparison, only the SOFA score variables, nasal catheter (NC), and mechanical ventilation (MV) days, had a moderate effect on Cohen's *d*, while the BF_{10} presents anecdotal evidence (Table S2, SI section). Therefore, it was concluded that the evaluated parameters are unsuitable for use as a prognostic model concerning the outcome of patients infected with COVID-19. However, since some parameters related to

Ery presented the statistical difference between COVID-19 and control patients, we investigated the functional and morphological states of the Ery to understand the possible influence on the disease.

Indeed, a few comparative (case-control) studies have addressed infection with SARS-CoV-2 and its effects on Ery function.[38] Thus, our results provide complementary information and insights into this relevant topic. Initially, in the Ery analysis, a decrease in O_2 uptake and reduction in antioxidant enzyme (SOD, CAT, and GPx) activity in COVID-19 patients was observed compared to control, corroborating that infection generally leads to an immune response mediated by ROS.[21] Moreover, the compromising of Ery caused by ROS is well-established; for instance, the Ery from fishermen who inhabits an environment exposed to Hg in the water had an altered redox status based on SOD and GPx as a reduction in O_2 uptake capacity.[14] Recently, our group published that human Ery, when exposed to a mercury compound, has some functional and structural changes, as seen in the present study.[12] Thus, based on O_2 uptake results, we investigated biophysical changes of Hb for COVID-19 patients.

Computational and sequencing genetics studies reported a new pathophysiological hypothesis caused by SARS-CoV-2 related to Hb dysfunction and tissue iron overload. Wenzhong and Hualan,[39] inferred that the virus inhibits the metabolism of heme by binding to the beta chains of hemoglobin through surface glycoproteins, facilitating iron removal.[40] The results of biophysical interaction studies of the Hb with model ligands (FA and QU) and conformational parameters indicated changes in the native protein (control) structure compared to COVID-19 patients. Therefore, the structural Hb alteration compromises the metabolic conditions and O_2 binding capacity of COVID-19 patients, leading to hypoxemia.[41-43]

Agreeing with the low capacity for oxygen transport by COVID-19 patients, Raman spectroscopy showed some remarkable differences between the groups. This technique uses light scattering, leading to a specific vibration that changes biomolecules.[11] Porphyrin ring and amino acid chains presented with alterations in Hb and structural changes in the membrane lipids of Ery using the 785 nm excitation laser.[44]

Finally, AFM presented changes in the morphological and mechanical properties of Ery in COVID-19 patients. The increase in Young's modulus of Ery can arise from changes in the membranes, leading to their stiffening. These results follow Raman spectroscopy data since we found structural changes in membrane lipids related to a decrease in fluidity, thus corroborating the higher Young's modulus in COVID-19 patients compared to the control.

Conclusions

Finally, from this data, it is valid to state that COVID-19 somehow leads to structural, functional, and morphological damage in human Ery. This impairment mainly affects Hb in its primary function of binding to oxygen, which may be one of the factors that aggravate respiratory problems that have more pronounced manifestations in COVID-19 patients compared to control patients.

Supplementary Information

Supplementary data (Tables S1-S4 and Figures S1-S4) are available free of charge at http://jbcs.sbq.org.br as PDF file.

Acknowledgments

Author Contributions

Marcos Sales and Eloisa Tanabe were responsible for investigation, formal analysis, writing original draft; Thamilla Maciel, Maria Tavares, Juliana Leal, Larissa Pinto, Keyla Pires, Elaine Silva, Samuel Souza for investigation; Jorge Coelho, Eduardo Fonseca, Thiago Fragoso, Thiago Aquino, Alexandre Borbely, Uéslen Rocha for conceptualization and methodology; Ana Catarina Leite and Josué C. Santos for conceptualization, methodology, supervision, funding acquisition.

References

1. Abboud, H.; Abboud, F. Z.; Kharbouch, H.; Arkha, Y.; el Abbadi, N.; el Ouahabi, A.; *World Neurosurg.* **2020**, *140*, 49. [Crossref]

2. Azevedo, R. B.; Botelho, B. G.; de Hollanda, J. V. G.; Ferreira, L. V. L.; de Andrade, L. Z. J.; Oei, T. S.; Mello, S. S. M. L.; Muxfeldt, E. S.; *J. Hum. Hypertens.* **2021**, *35*, 4. [Crossref]

3. Khadke, S.; Ahmed, N.; Ahmed, N.; Ratts, R.; Raju, S.; Gallogly, M.; de Lima, M.; Sohail, M. R.; *Virol. J.* **2020**, *17*, 154. [Crossref]

4. Mahmudpour, M.; Roozbeh, J.; Keshavarz, M.; Farrokhi, S.; Nabipour, I.; *Cytokine* **2020**, *133*, 155151. [Crossref]

5. Lee, Y.; Min, P.; Lee, S.; Kim, S.-W.; *J. Korean Med. Sci.* **2020**, *35*, 174. [Crossref]

6. Al-Samkari, H.; Karp Leaf, R. S.; Dzik, W. H.; Carlson, J. C. T.; Fogerty, A. E.; Waheed, A.; Goodarzi, K.; Bendapudi, P. K.; Bornikova, L.; Gupta, S.; Leaf, D. E.; Kuter, D. J.; Rosovsky, R. P.; *Blood* **2020**, *136*, 489. [Crossref]

7. Taneri, P. E.; Gómez-Ochoa, S. A.; Llanaj, E.; Raguindin, P. F.; Rojas, L. Z.; Roa-Díaz, Z. M.; Salvador, D.; Groothof, D.; Minder, B.; Kopp-Heim, D.; Hautz, W. E.; Eisenga, M. F.; Franco, O. H.; Glisic, M.; Muka, T.; *Eur. J. Epidemiol.* **2020**, *35*, 763. [Crossref]

8. Guan, X.; Zhang, B.; Fu, M.; Li, M.; Yuan, X.; Zhu, Y.; Peng, J.; Guo, H.; Lu, Y.; *Ann. Med.* **2021**, *53*, 257. [Crossref]

9. Revin, V. V.; Balykova, L. A.; Radaeva, O. A.; Shchapov, V. V.; Revina, E. S.; Pinyaev, S. I.; Kostina, Yu, A.; Kozlov, E. D.; *Bull. Exp. Biol. Med.* **2022**, *173*, 46. [Crossref]

10. Kronstein-Wiedemann, R.; Stadtmüller, M.; Traikov, S.; Georgi, M.; Teichert, M.; Yosef, H.; Wallenborn, J.; Karl, A.; Schütze, K.; Wagner, M.; El-Armouche, A.; Tonn, T.; *Stem Cell Rev. Rep.* **2022**, *18*, 1809. [Crossref]

11. Drescher, D.; Büchner, T.; McNaughton, D.; Kneipp, J.; *Phys. Chem. Chem. Phys.* **2013**, *15*, 5364. [Crossref]

12. Sales, M. V. S.; da Silva Filho, R. C.; Silva, M. M.; Rocha, J. L.; Freire, R. O.; Eloiza, E. L.; Silva, E. C. O.; Fonseca, E. J. S.; Figueiredo, I. M.; Rocha, U.; Santos, J. C. C.; Leite, A. C. R.; *J. Trace Elem. Med. Biol.* **2022**, *71*, 126928. [Crossref]

13. Silva, M. M.; Dantas, M. D. A.; da Silva-Filho, R. C.; Sales, M. V. S.; Xavier, J. A.; Leite, A. C. R.; Goulart, M. O. F.; Grillo, L. A. M.; Barros, W. A.; Fátima, Â.; Figueiredo, I. M.; Santos, J. C. C.; *Int. J. Biol. Macromol.* **2020**, *154*, 661. [Crossref]

14. Silva-Filho, R.; Santos, N.; Santos, M. C.; Nunes, Á.; Pinto, R.; Marinho, C.; Lima, T.; Fernandes, M. P.; Santos, J. C. C.; Leite, A. C. R.; *Ecotoxicol. Environ. Saf.* **2021**, *219*, 112337. [Crossref]

15. von Elm, E.; Altman, D. G.; Egger, M.; Pocock, S. J.; Gøtzsche, P. C.; Vandenbroucke, J. P.; *J. Clin. Epidemiol.* **2008**, *61*, 344. [Crossref]

16. Liu, S.; Yao, N.; Qiu, Y.; He, C.; *Am. J. Emerg. Med.* **2020**, *38*, 2074. [Crossref]

17. Singer, A. J.; Ng, J.; Thode, H. C.; Spiegel, R.; Weingart, S.; *Ann. Emerg. Med.* **2017**, *69*, 475. [Crossref]

18. Xiling, G.; Yin, C.; Ling, W.; Xiaosong, W.; Jingjing, F.; Fang, L.; Xiaoyan, Z.; Yiyue, G.; Ying, C.; Lunbiao, C.; Liubo, Z.; Hong, S.; Yan, X.; *Sci. Rep.* **2021**, *11*, 2418. [Crossref]

19. Bradford, M. M.; *Anal. Biochem.* **1976**, *72*, 248. [Crossref]

20. Ellman, G. L.; *Arch. Biochem. Biophys.* **1959**, *82*, 70. [Crossref]

21. Misra, H. P.; Fridovich, I.; *J. Biol. Chem.* **1972**, *247*, 3170. [Crossref]

22. Aebi, H. In *Methods in Enzymology*, vol. 105; Kaplan, N. P.; Colowick, N. P.; Sies, H., eds.; Academic Press: London, 1984, p. 121. [Crossref]

23. Masternak, J.; Zienkiewicz-Machnik, M.; Łakomska, I.; Hodorowicz, M.; Kazimierczuk, K.; Nosek, M.; Majkowska-

Młynarczyk, A.; Wietrzyk, J.; Barszcz, B.; *Int. J. Mol. Sci.* **2021**, *22*, 7286. [Crossref]

24. de Lyra, A. C. F.; Silva, A. L. S.; dos Santos, E. C. L.; López, A. M. Q.; da Silva, J. C. S.; Figueiredo, I. M.; Santos, J. C. C.; *Spectrochim. Acta, Part A* **2020**, *228*, 117747. [Crossref]

25. Matsushita, S.; Nishi, K.; Iwao, Y.; Ishima, Y.; Watanabe, H.; Taguchi, K.; Yamas, K.; Maruyama, T.; Otagiri, M.; *Biol. Pharm. Bull.* **2017**, *40*, 1813. [Crossref]

26. Horcas, I.; Fernández, R.; Gómez-Rodríguez, J. M.; Colchero, J.; Gómez-Herrero, J.; Baro, A. M.; *Rev. Sci. Instrum.* **2007**, *78*, 013705. [Crossref]

27. Burnham, N. A.; Chen, X.; Hodges, C. S.; Matei, G. A.; Thoreson, E. J.; Roberts, C. J.; Davies, M. C.; Tendler, S. J. B.; *Nanotechnology* **2002**, *14*, 1. [Crossref]

28. Quintana, D. S.; Williams, D. R.; *BMC Psychiatry* **2018**, *18*, 178. [Crossref]

29. Wagenmakers, E. J.; Marsman, M.; Jamil, T.; Ly, A.; Verhagen, J.; Love, J.; Selker, R.; Gronau, Q. F.; Šmíra, M.; Epskamp, S.; Matzke, D.; Rouder, J. N.; Morey, R. D.; *Psychon. Bull. Rev.* **2017**, *25*, 35. [Crossref]

30. Cohen, J. A.; *Psychol. Bull.* **1992**, *112*, 155. [Crossref]

31. Bortolotti, A.; Wong, Y. H.; Korsholm, S. S.; Bahring, N. H. B.; Bobone, S.; Tayyab, S.; van de Weert, M.; Stella, L.; *RSC Adv.* **2016**, *6*, 112870. [Crossref]

32. Cao, J.; Li, C.; Liu, R.; Liu, X. R.; Fan, Y.; Deng, Z. Y.; *Food Anal. Methods* **2017**, *10*, 649. [Crossref]

33. Santos, J. C. N.; da Silva, I. M.; Braga, T. C.; Fátima, Â.; Figueiredo, I. M.; Santos, J. C. C.; *Int. J. Biol. Macromol.* **2018**, *113*, 1032. [Crossref]

34. Herold, T.; Jurinovic, V.; Arnreich, C.; Lipworth, B. J.; Hellmuth, J. C.; von Bergwelt-Baildon, M.; Klein, M.; Weinberger, T.; *J. Allergy Clin. Immunol.* **2020**, *146*, 128. [Crossref]

35. Lenka, J.; Chhabria, M. S.; Sharma, N.; Tan, B. E.-X.; Boppana, L. K. T.; Enugopal, S.; Sondhi, D. S.; *J. Community Hosp. Intern. Med. Perspect.* **2020**, *10*, 491. [Crossref]

36. Cheng, L.; Li, H.; Li, L.; Liu, C.; Yan, S.; Chen, H.; Li, Y.; *J. Clin. Lab. Anal.* **2020**, *34*, e23618. [Crossref]

37. Thomas, T.; Stefanoni, D.; Dzieciatkowska, M.; Issaian, A.; Nemkov, T.; Hill, R. C.; Francis, R. O.; Hudson, K. E.; Buehler, P. W.; Zimring, J. C.; Hod, E. A.; Hansen, K. C.; Spitalnik, S. L.; D'Alessandro, A.; *J. Proteome Res.* **2020**, *19*, 4455. [Crossref]

38. Nader, E.; Nougier, C.; Boisson, C.; Poutrel, S.; Catella, J.; Martin, F.; Charvet, J.; Girard, S.; Havard-Guibert, S.; Martin, M.; Rezigue, H.; Desmurs-Clavel, H.; Renoux, C.; Joly, P.; Guillot, N.; Bertrand, Y.; Hot, A.; Dargaud, Y.; Connes, P.; *Am. J. Hematol.* **2022**, *97*, 283. [Crossref]

39. Wenzhong, L.; Hualan, L.; *ChemRxiv* **2020**. [Link] accessed in April 2020.

40. Wagener, F. A. D. T. G.; Pickkers, P.; Peterson, S. J.; Immenschuh, J.; Abraham, N. G.; *Antioxidants* **2020**, *9*, 540. [Crossref]

41. Majeed, A.; Ashraf Shajar, M.; *Anaesth., Pain Intensive Care* **2020**, *24*, 9. [Crossref]

42. Cavezzi, A.; Troiani, E.; Corrao, S.; *Clin. Pract.* **2020**, *10*, 1271. [Crossref]

43. Li, N.; Li, S. X.; Guo, Z. Y.; Zhuang, Z. F.; Li, R.; Xiong, K.; Chen, S. J.; Liu, S. H.; *J. Photochem. Photobiol., B* **2012**, *112*, 37. [Crossref]

44. Ahlawat, S.; Kumar, N.; Uppal, A.; Gupta, P. K.; *J. Biophotonics* **2017**, *10*, 415. [Crossref]